Progress In Electromagnetics Research M, Vol. 97, 45–56, 2020

NLOS Target Localization with an L-Band UWB Radar via Grid Matching

Huagui Du, Chongyi Fan*, Zhen Chen, Chun Cao, and Xiaotao Huang

Abstract—This paper considers utilizing radar multipath returns to locate a target hidden behind a corner. A novel target localization algorithm based on grid matching is proposed for non-line of sight (NLOS) environment. The algorithm first establishes a multipath propagation model based on real data from an L-band ultra-wideband (UWB) radar. Then, it calculates the times of arrival (TOAs) of each grid based on the multipath propagation model and matches the grid which is closest to the measured TOAs of round-trip multipath returns. Both simulation and real-data experiment results validate the effectiveness of the multipath model and the proposed localization algorithm.

1. INTRODUCTION

Localization targets hidden behind a corner have aroused wide interest in both military and civil security fields [1, 2]. As in battle reconnaissance and city monitoring, it is not expected to expose the first responders under any threat in dangerous scenes, which may meet during the action like anti-terrorism or fire rescue. However, conventional optical surveillance device mostly works in line of sight (LOS), which is unsuitable in adverse atmospheric conditions. The existing research results show that a simple portable radar called "around-the-corner" radar (ACR) has the ability of NLOS targets detection and localization, which regards multipath signals as useful signals rather than interference. It can extract the target information from the NLOS multipath returns, which can be used to look behind corners [3–7]. The feasibility of ACR has been demonstrated by exploiting the multipath specular reflection, diffraction, and even diffuse reflection [8–15].

The application research of radar multipath signals originated in the DARPA's Multipath Exploitation Radar program [16, 17]. In the early stages, researchers mainly focused on the feasibility analysis of obtaining NLOS target information from multipath signals, followed by the multipath detection. In recent years, the focus turns to exploiting multipaths to locate NLOS targets [18–25]. The NLOS localization algorithms can be divided into two types with respect to single and multiple multipath signals. The first type utilizes only one single robust multipath signal, which is very common in millimeter wave radar(MMW). In [18], the localization algorithm with single multipath return is proposed based on phased comparison among the multiple channels. In [19], positioning the target is realized by a synthetic bistatic MMW radar. However, these methods are not suitable for low-frequency radars which usually meet multiple kinds of multipaths at the same time. To solve this problem, the second type focuses on extracting target information from multiple multipath signals. Zetik et al. proposed a NLOS target localization method that considers a one-bounce reflection and a diffraction path, ignoring more-bounce reflection paths [20]. In [21], a localization method is provided based on the assumption that all kinds of multipath signals can be received and extracted. Without this ideal assumption, Thai et al. [22] and Rabaste et al. [23] proposed a detection-localization algorithm based on the subspace filter matching and ray-tracing, which is verified by real experiments. Their work has

Received 18 July 2020, Accepted 11 September 2020, Scheduled 29 September 2020
* Corresponding author: Chongyi Fan (chongyifan@nudt.edu.cn).
The authors are with the College of Electronic Science and Technology, National University of Defense Technology, China.

good positioning accuracy but takes time. In addition, according to the idea of path matching, several NOLS localization algorithms have been proposed [24–26]. The core part of positioning is to correctly match the measured TOAs with the propagation paths in [24, 25], and the algorithm in [26] requires that all propagation paths are detected and associated with walls. However, it is very difficult for all paths to be successfully detected and correctly matched in real data.

To avoid matching the measured TOAs with propagation paths and considering computational efficiency, a novel NLOS target localization algorithm based on grid matching is proposed in this paper. This algorithm takes two or more-bounce reflection paths into account and only extracts the measured TOAs, omitting the matching between the measured TOAs and the propagation paths by meshing method. The higher the number of TOAs exists, the better the localization performance is. Actually, by controlling the size of the mesh, the proposed algorithm can cope with the case where some measured TOAs are missed, or the distance measurement error appears. In addition, the theoretical propagation distance can be calculated in advance for one scenario, which guarantees the real-time realization.

The rest of this paper is organized as follows. In Section 2, the multipath propagation model for an L-shaped corner is constructed. In Section 3, the proposed localization algorithm based on grid matching is introduced in detail. In the next section, the localization error is analyzed by simulation firstly, and then two real experiments will be carried out. Finally, Section 5 concludes this paper.

2. MULTIPATH MODELING

Consider a typical NLOS scenario of urban streets — an L-shaped corner with perpendicularly bent walls, as shown in Fig. 1. A local coordinate system with the x-axis parallel to the Wall-3 is established. The radar is placed at the origin of the local coordinate system, and the position is $\mathbf{R}_{tr} = [x_{tr}, y_{tr}]^T$. The corner formed by Wall-1 and Wall-3 is $\mathbf{C} = [x_c, y_c]^T$. L is the width of the aisle formed by Wall-1 and Wall-2, so the x-coordinates of Wall-1 and Wall-2 are x_c and $(x_c + L)$, respectively. Suppose that a concealed target $\mathbf{T} = [x_T, y_T]^T$ is located in the NLOS area indicated by shadow, and the scenario geometric structure is known as the priori knowledge. For example, the building layout can be obtained through other auxiliary tools, such as Lidar.

As shown in Fig. 1, the transmitted radar signals with great attenuation cannot directly propagate to the target $\mathbf{T}$ behind the corner due to the presence of the corner $\mathbf{C}$, while the multipath returns keep the signal energy. The research in [24, 25] shows that for an L-band UWB radar, four or more-

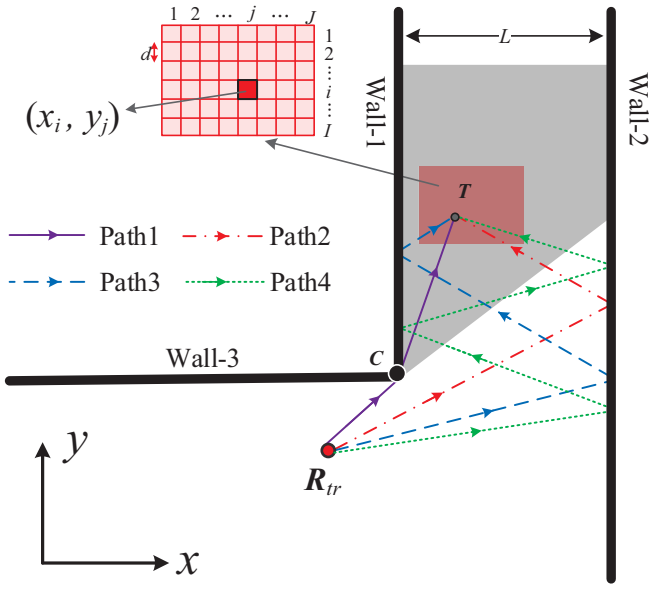

Figure 1. Multipath propagation model.

bounce reflection paths suffer from severe attenuation and cannot effectively provide target information. So four types single-trip propagation paths, named Path1, Path2, Path3, and Path4 (see Fig. 1), are considered in this paper. Specifically, Path1 represents the radar radiation signal which propagates to the potential target **T** by diffraction, and Path2, Path3, and Path4 represent single-trip propagation paths by one-bounce, two-bounce, and three-bounce reflection due to Wall-1 and Wall-2, respectively. Because both of the transmitted and received signals may pass by these four paths, the receiver can capture ten combinations of different round-trip propagation paths for an L-band UWB radar. Stacking all these round-trip propagation paths in a vector **P**, we have:

$$\begin{aligned} \mathbf{P} &= [p_{11},\ p_{12},\ p_{mn},\ \ldots,\ p_{44}]^T, \\ & m \le n, \quad m, n \in \{1, 2, 3, 4\}, \end{aligned} \tag{1}$$

where p_{mn} denotes the round-trip propagation path combined with Path-m transmission and Path-n reception. In this paper, p_{mn} and p_{nm} are treated as the same path.

The propagation distances of different propagation paths in Equation (1) are represented in a vector **R**, which can be expressed as:

$$\begin{aligned} \mathbf{R} &= [r_{11},\ r_{12},\ r_{mn},\ \ldots,\ r_{44}]^T, \\ & m \le n, \quad m, n \in \{1, 2, 3, 4\}, \end{aligned} \tag{2}$$

and r_{mn} represents the round-trip propagation distance of the path p_{mn}.

Assume that the scenario geometric structure is known, and the specular reflection is stronger than other reflections. Therefore, **R** can be calculated theoretically as follows. Firstly, according to the principle of mirror symmetry and multipath propagation model in Fig. 1, the positions of virtual targets $\mathbf{S}_1$, $\mathbf{S}_2$, $\mathbf{S}_3$, and $\mathbf{S}_4$ generated by Path1, Path2, Path3, and Path4 can be obtained. Specifically, $\mathbf{S}_m$ can be calculated by:

$$\begin{cases} \mathbf{S}_1 = [x_1, y_1]^T = [x_T, y_T]^T, \\ \mathbf{S}_2 = [x_2, y_2]^T = [2\,(x_c + L) - x_T, y_T]^T, \\ \mathbf{S}_3 = [x_3, y_3]^T = [2\,(x_c + L) - 2x_c + x_T, y_T]^T, \\ \mathbf{S}_4 = [x_4, y_4]^T = [4\,(x_c + L) - 2x_c - x_T, y_T]^T. \end{cases} \tag{3}$$

Then, according to Fig. 1 and Eq. (3), the propagation distance r_m of the transmitting Path-m and the propagation distance r_n of the receiving Path-n can be calculated by:

$$r_m = \begin{cases} \|\mathbf{R}_{tr}\mathbf{C}\| + \|\mathbf{C}\mathbf{T}\|, & m = 1, \\ \|\mathbf{R}_{tr}\mathbf{S}_m\|, & m = 2, 3, 4, \end{cases} \tag{4}$$

and

$$r_n = \begin{cases} \|\mathbf{T}\mathbf{C}\| + \|\mathbf{C}\mathbf{R}_{tr}\|, & n = 1, \\ \|\mathbf{S}_n\mathbf{R}_{tr}\|, & n = 2, 3, 4, \end{cases} \tag{5}$$

where $\|\cdot\|$ denotes the Euclidean norm.

Finally, the distance r_{mn} of the round-trip propagation path can be obtained by:

$$r_{mn} = r_m + r_n \tag{6}$$

Consequently, considering all transmitting and receiving propagation paths, the distance vector **R** can be obtained.

3. THE PROPOSED ALGORITHM

In this section, the proposed NLOS localization algorithm is derived and explained in details. Furthermore, in order to facilitate understanding and application, the whole signal processing flow is given.

3.1. The Construction of Grid Matching Matrix

A classical NLOS scenario can be represented as an L-shaped corner as shown in Fig. 1. The received radar echo $z(t)$ is a superposition of multiple specular multipath returns, which is given by:

$$z(t) = \sum_{m=1}^{M} \sum_{n=1}^{N} \sigma_{mn} s\left[t - \tau_m\left(x_T, y_T\right) - \tau_n\left(x_T, y_T\right)\right] + w(t), \tag{7}$$

where M and N represent the numbers of transmitting and receiving paths, respectively; σ_{mn} is the complex reflection coefficient of the path p_{mn}; $s(t)$ represents the transmitted radar signal; $w(t)$ denotes the noise; and $\tau_m(x_T, y_T)$ and $\tau_n(x_T, y_T)$ respectively denote the time delay of transmitting Path-m and receiving Path-n for the target located at (x_T, y_T).

Theoretically, the TOAs of all paths in Eq. (1) can be obtained from the radar echo $z(t)$ through signal preprocessing techniques of MTI [20], FFT, and CA-CFAR [27]. However, due to the presence of interference and noise, some multipaths may be lost, and the real number of extracted TOAs may be less than the ideal value in Eq. (1). Stack all the extracted TOAs in a vector $\mathbf{T}_e$, and $\mathbf{T}_e = [\tau_1, \tau_2, \ldots \tau_Q]^T$. Thus the measured target range vector $\mathbf{R}_{measure}$ is given by:

$$\mathbf{R}_{measure} = c\mathbf{T}_e = [R_1, R_2, \ldots, R_q, \ldots, R_Q]^T, \tag{8}$$

where c represents the velocity of EM wave in the air, and Q is the number of extracted TOAs. For the L-band radar, Q usually does not exceed ten, because four or more-bounce reflection paths suffer severe attenuation and are ignored.

After obtaining the range vector $\mathbf{R}_{measure}$, the method of meshing the NLOS area is used to obtain target position. With this method, the calculation efficiency and positioning accuracy are guaranteed. The core principle of positioning is to construct a grid matching matrix through $\mathbf{R}_{measure}$ and theoretical propagation distance. Specifically, the construction of the grid matching matrix needs four steps:

Step 1: Divide the NLOS area to be detected into grids of $I \times J$. The spacing between grids is d, as shown in Fig. 1, which does not exceed the range resolution ΔR_u of the radar system. Here the central position of each grid is (x_i, y_j), and $i \in \{1, 2, \ldots, I\}, j \in \{1, 2, \ldots, J\}$.

Step 2: Calculate the theoretical distance vector $\mathbf{R}_{ij}$ of round-trip propagation paths for the potential target at the grid position (x_i, y_j). According to Eqs. (4), (5), and (6), $\mathbf{R}_{ij}$ can be expressed as:

$$\mathbf{R}_{ij} = \left[r_{11}^{ij}, r_{12}^{ij}, r_{mn}^{ij}, \ldots, r_{44}^{ij}\right]^T. \tag{9}$$

Step 3: Calculate the grid matching matrix. Specifically, we first initialize the grid matching matrix to $\mathbf{G}$:

$$\mathbf{G} = \begin{bmatrix} g_{11} & g_{12} & \cdots & g_{1J} \\ g_{21} & g_{22} & \cdots & g_{2J} \\ \vdots & \vdots & \vdots & \vdots \\ g_{I1} & g_{I2} & \cdots & g_{IJ} \end{bmatrix}. \tag{10}$$

and set the grid matching vector to $\mathbf{A}$:

$$\mathbf{A} = \left[A_{11,1}^{ij}, A_{12,1}^{ij}, \ldots, A_{mn,q}^{ij}, \ldots, A_{44,Q}^{ij}\right]_{10Q\times 1}^{T}. \tag{11}$$

where $A_{mn,q}^{ij}$ can be calculated by:

$$A_{mn,q}^{ij} = \left|r_{mn}^{ij} - R_q\right|, r_{mn}^{ij} \in \mathbf{R}_{ij}, R_q \in \mathbf{R}_{measure}. \tag{12}$$

Then, reconstruct the grid matching vector $\mathbf{A}$ to $\tilde{\mathbf{A}}$:

$$\tilde{\mathbf{A}} = \left[\tilde{A}_{11,1}^{ij}, \tilde{A}_{12,1}^{ij}, \ldots, \tilde{A}_{mn,q}^{ij}, \ldots, \tilde{A}_{44,Q}^{ij}\right]_{10Q\times 1}^{T}. \tag{13}$$

and $\tilde{A}_{mn,q}^{ij}$ can be obtained by:

$$\tilde{A}_{mn,q}^{ij} = \begin{cases} 1, A_{mn,q}^{ij} \le \Delta R_u, \\ 0, A_{mn,q}^{ij} > \Delta R_u. \end{cases} \tag{14}$$

At last, the element of g_{ij} in the grid matching matrix $\mathbf{G}$ is presented as follows:

$$g_{ij} = sum(\tilde{\mathbf{A}}), \tag{15}$$

where $sum(\tilde{\mathbf{A}})$ represents the sum of all elements in $\tilde{\mathbf{A}}$, and g_{ij} also represents the number of elements smaller than ΔR_u in vector $\mathbf{A}$.

Step 4: By repeating Steps 2 and 3 for all grids, the grid matching matrix will be obtained.

In summary, $\mathbf{G}$ can be obtained by acquiring the building layout, position of the radar, and measured TOAs. To calculate $\mathbf{G}$, a large amount of calculation is mainly derived from Equation (9). In order to improve real-time processing, $\mathbf{R}_{ij}$ can be calculated and stored in advance when the building layout is known. For the same scenario, this comparably time-consuming calculation only needs to calculate one time.

3.2. The Determination of Target Location

After the grid matching matrix $\mathbf{G}$ is obtained, the target $\mathbf{T}$ behind an L-shaped corner will be located. The positioning principle is that if grid (x_i, y_j) is the real target position, most of the measured range in Eq. (8) will be correctly matched ($A^{ij}_{mn,q} = 1$) by the theoretical distance vector in Eq. (9), and g_{ij} will reach the maximum.

In the ideal case, all multipath returns can be detected correctly by CA-CFAR with accurately radar ranging. If the spacing d is small enough, the position of the grid which has the largest element g_{ij} in $\mathbf{G}$ is the target position. However, in fact, there is not only one maximum value in $\mathbf{G}$. On the one hand, the number of propagation paths measured in practice is usually less than the theoretical value. On the other hand, due to the influence of noise and system errors, the measured round-trip propagation distance $\mathbf{R}_{measure}$ and theoretical distance $\mathbf{R}$ cannot be completely consistent. Thus, the larger values of $\mathbf{G}$ will be distributed in multiple grids and concentrated around grids which are near the target's real position. For a single target, elements with larger values in $\mathbf{G}$ will only appear in one area. Therefore, the target can be located by finding this area. In practice, we mainly need three steps to find this area:

Step 1: Obtain a binary grid matching matrix $\tilde{\mathbf{G}}$ by threshold detection T_{thre}, and $\tilde{g}_{ij}$ is given by:

$$\tilde{g}_{ij} = \begin{cases} 1, & g_{ij} \geq T_{thre}, \\ 0, & g_{ij} < T_{thre}. \end{cases} \tag{16}$$

It is worth pointing out that T_{thre} is related to the number of elements (P_{num}) in vector $\mathbf{R}_{measure}$ in Eq. (8). The selection of T_{thre} will be researched in the next section.

Step 2: Eliminate a small number of discrete points with the value of 1 in $\tilde{\mathbf{G}}$ by using the strel function, and strel function is an operation of morphological dilation and erosion.

Step 3: Extract the connected domains by bwlabel function. The connected domain with the largest area is denoted as S, and the real position of the target will be in the grid represented by S. Furthermore, the centroid of S is calculated as the position of the target $\mathbf{T}$, expressed as:

$$\mathbf{T} = [\hat{x}, \hat{y}]^T = cent(S), \tag{17}$$

where $(\hat{x}, \hat{y})$ represents the estimated position of the target, and $cent(\cdot)$ is the calculation of centroid.

Finally, in order to facilitate the understanding and application of the proposed algorithm, the flowchart of the algorithm is given, as shown in Fig. 2.

4. SIMULATION AND EXPERIMENTAL RESULTS

In this section, the localization performance will be analyzed under different conditions through numerical simulation. Furthermore, real data experiments are implemented to explain the processing steps and validate the effectiveness of the algorithm.

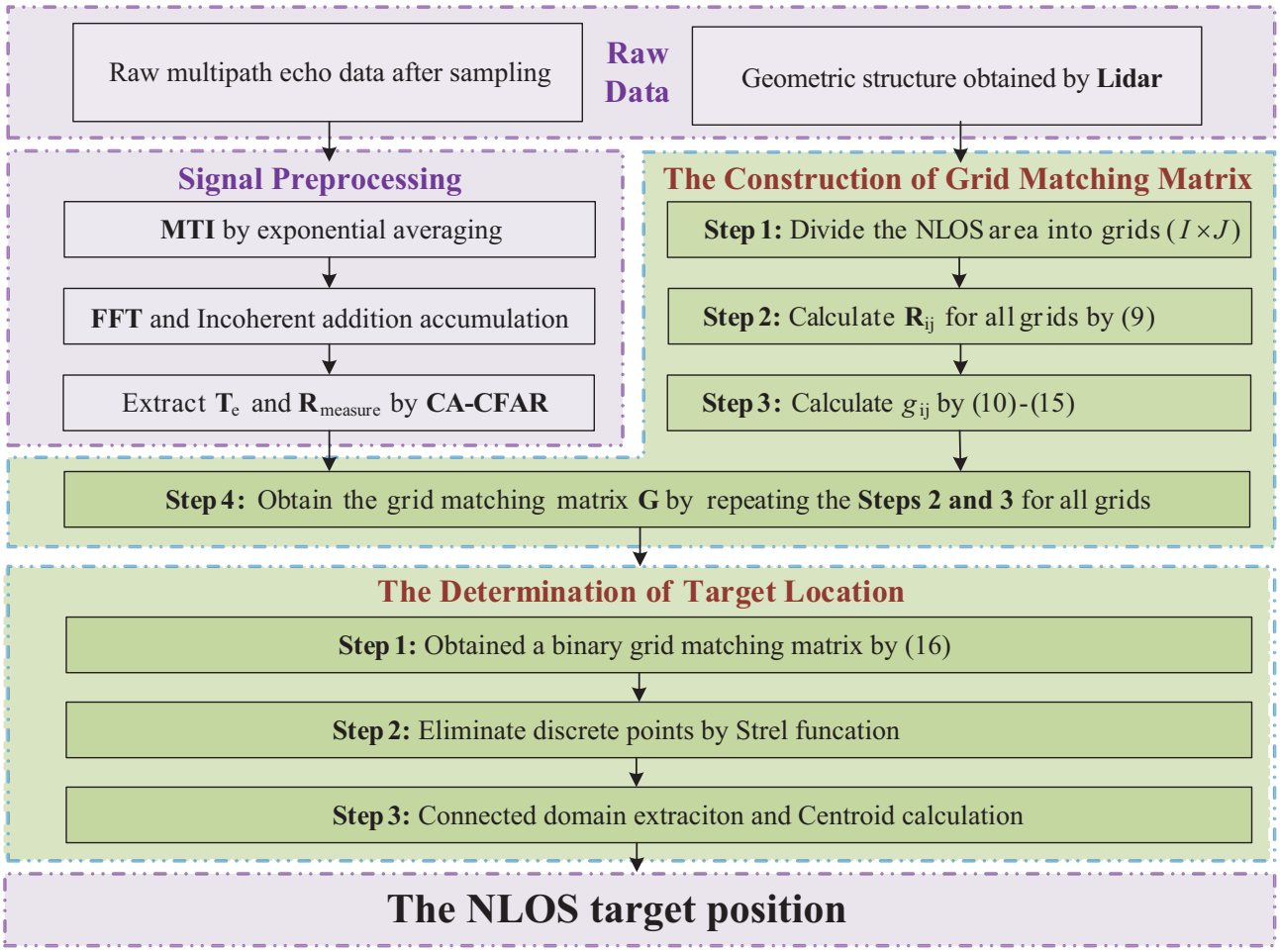

Figure 2. Block diagram of the proposed algorithm.

4.1. Performance Simulation

According to Section 3.2, it can be known that the proposed algorithm depends on the detection threshold T_{thre}, and choosing a suitable T_{thre} is essential for precise positioning. In the ideal case, the maximum value in $\mathbf{G}$ is (P_{num}), and the grid position where the maximum value is located is the true position of the target. Thus, selecting P_{num} as T_{thre} can correctly extract the target position information. However, if the maximum value P_{num} is selected as T_{thre}, the area of the extracted connected domain S may be small, and S may be eliminated by the strel function. Therefore, in order to prevent the target from being eliminated and to ensure the effectiveness of the algorithm when the ranging error occurs, the area of the connected domain S is expanded by selecting $(P_{num}-1)$ or $(P_{num}-2)$ as T_{thre}.

In order to quantitatively illustrate the positioning performance, the influence of the number of TOAs (P_{num}), binary detection threshold T_{thre}, and ranging error (ΔR_{error}) are considered. The grid size d and range resolution ΔR_u are 0.05 m and 0.01 m, respectively. In addition, we assume that the ranging error follows a Gaussian distribution with mean ΔR_{error}, and the ranging error ΔR_{error} considered in the simulation is 0 to 0.5 m. This is because the system with larger ΔR_{error} is not suitable for the narrow NLOS scenario, such as corridors and parking lot entrances. For these scenes, the area of interest to be detected is small, only high-precision positioning results can provide effective target information, which is convenient for the operator to make decisions.

For selected P_{num}, T_{thre}, and ΔR_{error}, 300 independent Monte Carlo simulation experiments are performed, and the localization error is used to evaluate the performance. Specifically, the localization

error is given by:

$$Error = \frac{\sum_{k=1}^{Mon} \sqrt{(\hat{x}_k - x_T)^2 + (\hat{y}_k - y_T)^2}}{Mon} \tag{18}$$

where $(\hat{x}_k, \hat{y}_k)$ represents the estimated target position from the k-th Monte Carlo simulation experiment; (x_T, y_T) is the real position of the target; and Mon denotes the number of Monte Carlo simulation experiments.

Figures 3(a) and (b) show the localization error results when the detection threshold T_{thre} is $(P_{num} - 1)$ and $(P_{num} - 2)$, respectively. Comparing Figures 3(a) with (b), it can be seen that the proposed algorithm has better stability when T_{thre} is $(P_{num} - 2)$. Actually, it has good positioning performance when P_{num} is more than 5, and ΔR_{error} is less than 0.3 m (see Fig. 3(b)). This is because the larger elements in $\mathbf{G}$ can be accurately extracted by T_{thre} and bwlabel function in this case. On the contrary, when ΔR_{error} has a larger value and serious loss of paths, the connected domain containing the real position of the target cannot be accurately obtained. Therefore, a large positioning error will occur.

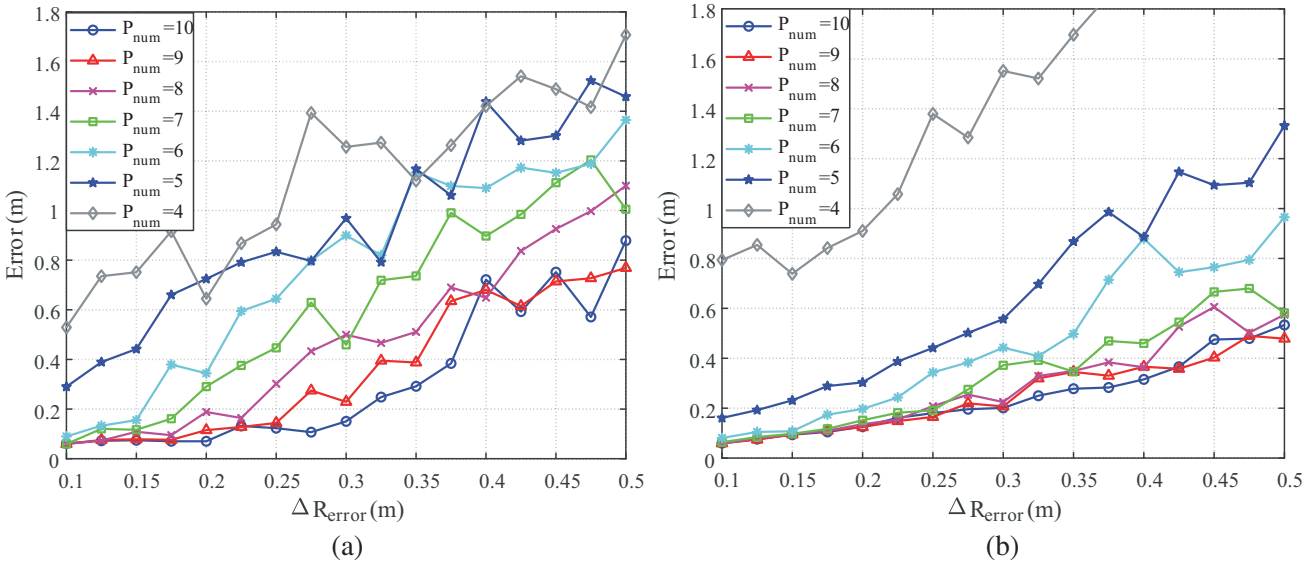

Figure 3. The localization error results. (a) $T_{thre} = P_{num} - 1$. (b) $T_{thre} = P_{num} - 2$.

Consequently, in the case of unknown ranging error ΔR_{error}, in order to seek the stability of the algorithm, it is usually best to choose $(P_{num} - 2)$ as the binary detection threshold T_{thre}.

4.2. Real Data Experiments

To validate the proposed localization algorithm experimentally, real data are collected by using an L-band UWB radar with the step-frequency continuous wave (SFCW) signal. An L-shaped parking lot entrance (see Fig. 4) was chosen as the experiment environment. Fig. 4(a) shows the optical image of the scene, and Fig. 4(b) shows the 2-D plane obtained by Lidar. The position of the corner is $\mathbf{C} = [1.0, 0.5]^T$, and the width of entrance is 5.4 m. The radar system is placed at 1.4 m high from the ground, and the antenna array is directed toward Wall-2 (only one receiving channel is used in this paper). Specifically, the detailed parameters of the radar system are listed in Table 1. Two experiments considering different target move conditions are performed.

Experiment 1: An experiment considering the case of micro-motion NLOS target is carried out. During the data collection, a person stood at the position $\mathbf{T} = [3.5, 2.5]^T$ (see Fig. 4(b)), and he was swaying back and head with a small range. According to the proposed algorithm, the processing results

Table 1. The key parameters of the SFCW radar.

Parameters	Value	Parameters	Value
Bandwidth	1.5 GHz	Number of Steps	750
Step Frequency	2 MHz	Distance ambiguity	75 m

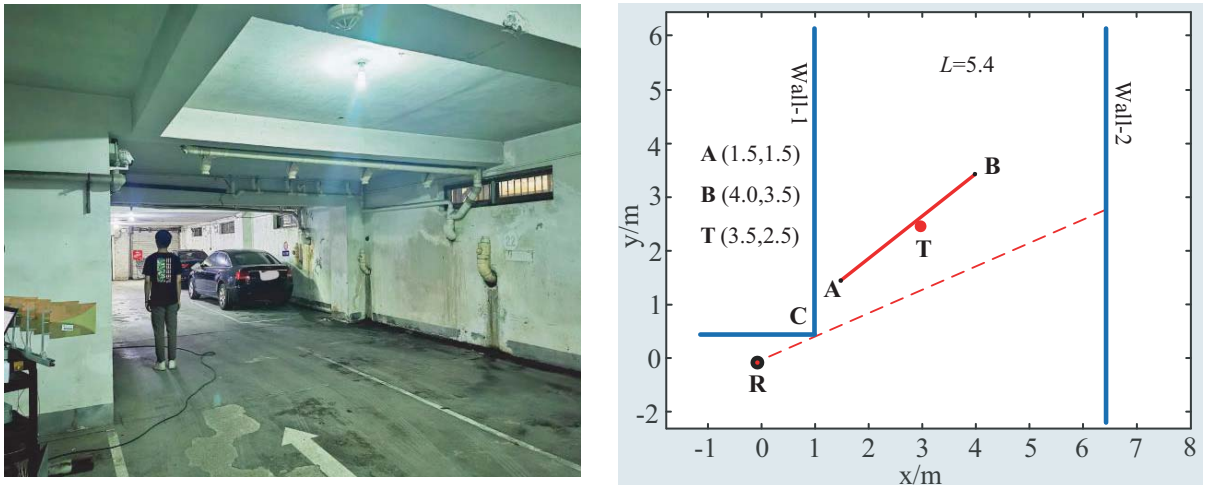

(a) (b)

Figure 4. Experiment scenario. (a) The real experiment scenario. (b) 2-D plane of experiment scenario.

of the multipath returns are shown in Fig. 5. Firstly, the signal preprocessing technology is employed to extract TOAs, and the result of a typical period is shown in Fig. 5(a). Obviously, six multipath signals and their distances can be obtained, and the real propagation paths have been marked by arrows. Secondly, mesh the area with x-coordinates from 1.0 m to 6.4 m and y-coordinates from 0.5 m to 6 m. The cell size d is 0.01 m. According to Section 3.1, the grid matching matrix $\mathbf{G}$ is obtained, as shown in Fig. 5(b). It can be discovered that the maximum value in $\mathbf{G}$ does not exceed 6, and the larger values are concentrated around the real position of the target. Then, when the threshold is $(P_{num}-1)$, according to Eq. (16), the binary grid matching matrix $\tilde{\mathbf{G}}$ is obtained, as shown in Fig. 5(c). Obviously, there are some discrete points in $\tilde{\mathbf{G}}$, which will lead to ambiguous positioning. Thus, the strel and bwlabel functions are utilized, and the result is shown in Fig. 5(d). Finally, the target position can be obtained by calculating the centroid of the connected domain, and the result is $\mathbf{T} = [3.495, 2.595]^T$. It can be seen that the micro-motion target is located successfully.

Next, the grid matching and path matching [24] localization algorithms are applied to the data of 25 periods, respectively. The results are shown in Fig. 6. It can be seen that the localization results of grid matching are closer to the real target position than the results of path matching, and the average localization error is 0.2689 m. However, the average localization error of the path matching algorithm is 0.584 m. When the path cannot be matched correctly, the positioning result seriously deviates from the real target position, and the maximum localization error is about 2 m (see Fig. 6(b)). In addition, the calculation times of the two algorithms are compared through simulation in the same NLOS scene, and the results are shown in Table 2. It shows that the grid matching algorithm has better real-time performance, and path matching localization algorithm needs a longer calculation time. This is mainly because the principle of the path matching algorithm is to cyclically match the theoretical propagation paths with the extracted TOAs. In the best case, only one cycle matching is required. At this time, the calculation time is shown in Table 2. In the worst case, C_N^2 cycles matching is required, and N represents the number of theoretical propagation paths.

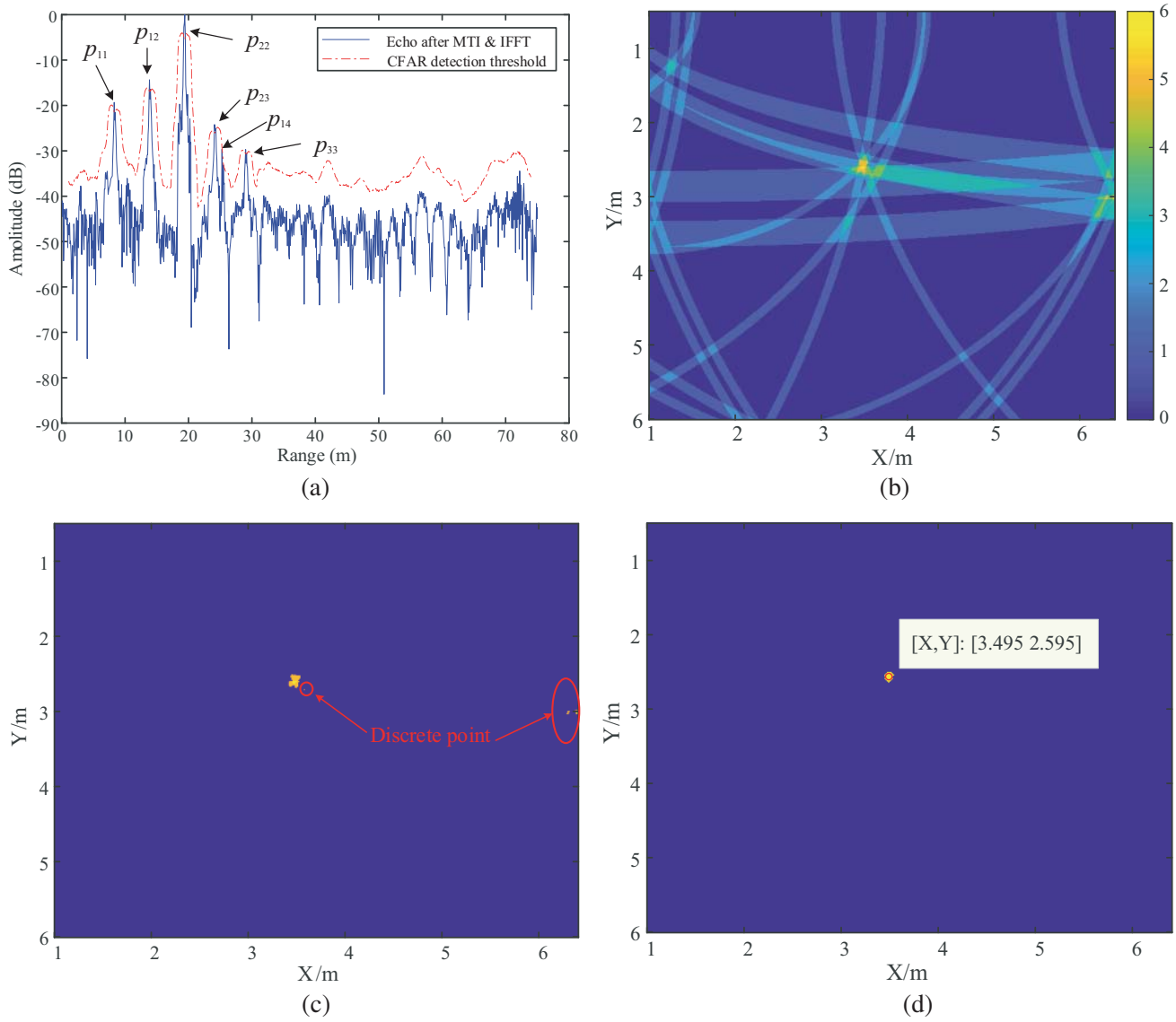

Figure 5. The multipath returns processing steps and results. (a) TOAs extraction results. (b) The grid matching matrix. (c) The binary grid matching matrix. (d) Positioning results.

Table 2. Comparison of calculation time under different number of paths and localization methods.

Path Number:	10	9	8	7	6	5	4
Grid Matching:	1.509 s	1.390 s	1.326 s	1.221 s	1.133 s	1.049 s	0.961 s
Path Matching (Min):	92.391 s	66.955 s	52.189 s	37.341 s	27.393 s	19.068 s	10.788 s

In summary, the algorithm proposed in this paper has better positioning accuracy and real-time performance, which can better meet the needs of practical applications such as urban anti-terrorism.

Experiment 2: For the case of moving target, a total of 100 periods of moving target data is collected from $\mathbf{A} = [1.5, 1.5]^T$ to $\mathbf{B} = [4.0, 3.5]^T$ as a straight line (see Fig. 4(b)). Fig. 7(a) shows the results of signal preprocessing for all periods raw data. It is noted that most of the multipath propagation paths aforementioned appear with strong amplitudes and can be detected in most time

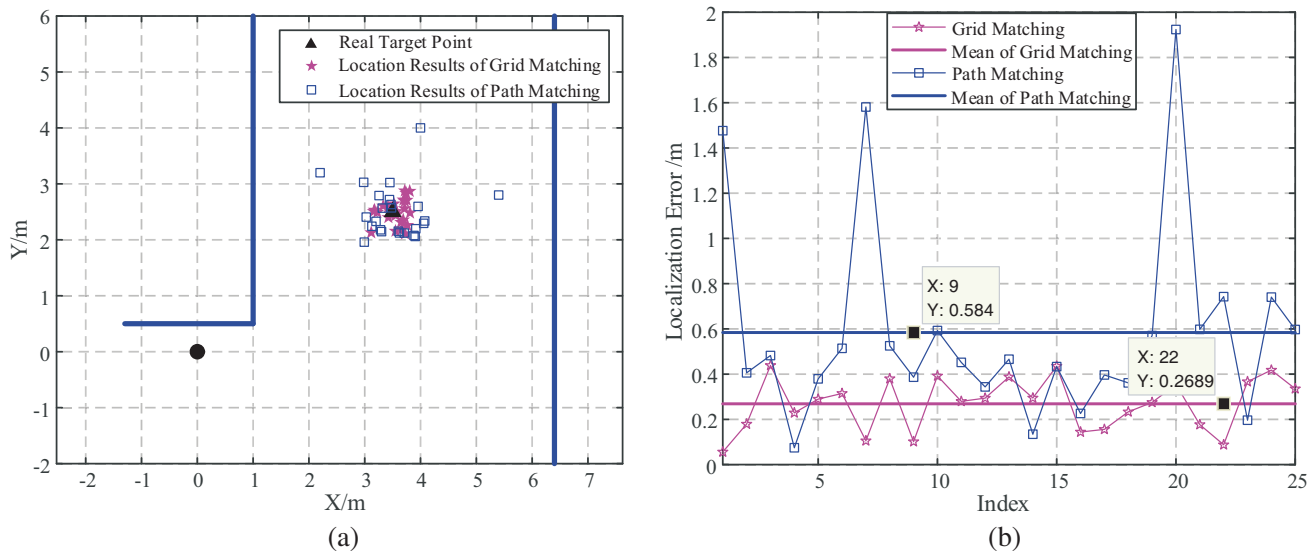

Figure 6. Micro-motion target experiment results. (a) The localization results. (b) The localization error.

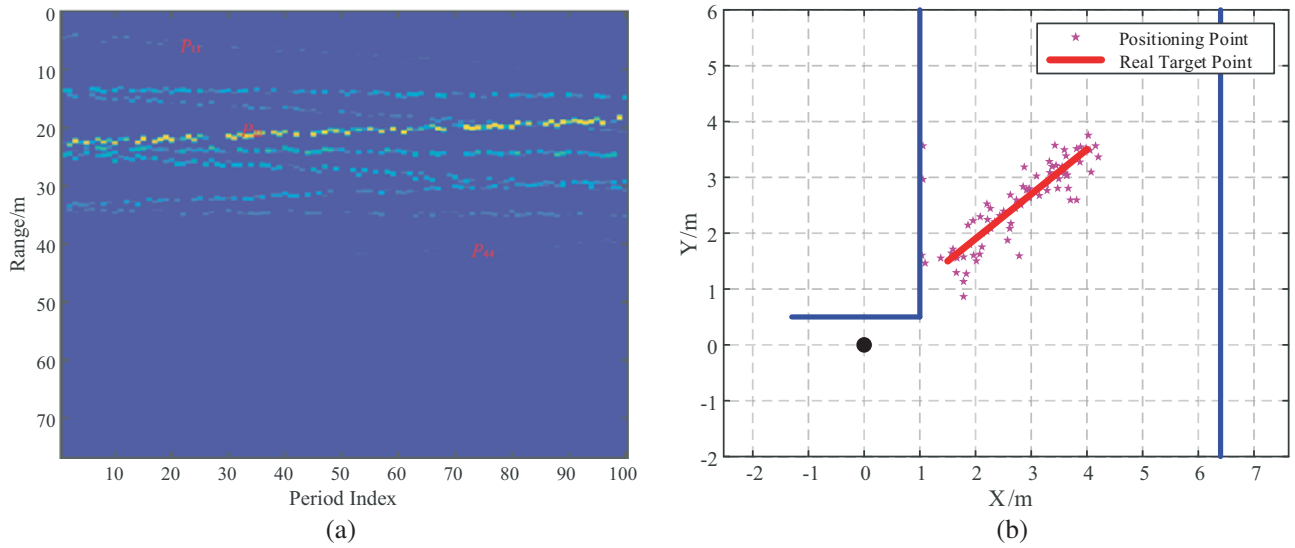

Figure 7. Moving target experiment results. (a) The results of signal preprocessing on the raw data. (b) Moving target localization results.

periods. In particular, multipath signals generated by diffraction and three-bounce reflection suffer severe attenuation, and one-bounce reflection paths are stable with strong amplitudes.

The position of the target, as shown in Fig. 7(b), can be obtained through repeating the signal processing flow in Fig. 2. It is worth pointing out that in order to obtain an accurate target position, the data of the periods with a smaller P_{num} ($P_{num} < 5$) are eliminated. Although it can be seen that measurement trajectory has a fluctuation compared with the real trajectory, which is caused by the effect of noise and range measurement error, it is acceptable in practice. Therefore, the proposed algorithm successfully locates the moving target based on the L-band UWB radar.

5. CONCLUSIONS

This paper focuses on the localization problem of an NLOS target. First of all, the multipath propagation model under an L-band radar is established. Then, considering the calculation efficiency and positioning accuracy, a novel target localization algorithm based on TOAs to construct the grid matching matrix is proposed. The performance of the proposed algorithm is analyzed by simulation data and shows that it has good positioning performance when the number of propagation paths is more than 5, with the ranging error less than 0.3 m. Meanwhile, the experimental results have also illustrated the effectiveness of the proposed algorithm. Consequently, this paper solves the problem of NLOS target location through grid matching. The proposed algorithm has good positioning accuracy and real-time performance, which can better meet the needs of practical applications such as urban anti-terrorism.

In the future, we plan to extend the proposed algorithm to NLOS multi-target positioning, and the localization method under inaccurate or unknown building layout will be researched.

ACKNOWLEDGMENT

This work was supported in part by the National Defense Pre-Research Foundation of China under Grant 6140413020406.

REFERENCES

1. Deiana, D., A. S. Kossen, and W. L. van Rossum, "Multipath exploitation in an urban environment using a mimo surveillance radar," *Proc. 11-th International Radar Sumposium*, 1–4, Vilnius, Lithuania, 2010.
2. Setlur, P. and M. Amin, "Multipath model and exploitation in through-the-wall radar and urban sensing," *IEEE Trans. Geosci. Remote Sens.*, Vol. 49, No. 10, 4021–4034, 2011.
3. Tahmoush, D., J. Silvious, and B. Bender, "Radar surveillance in urban environments," *Proceedings of the IEEE International Radar Conference*, 220–225, 2012.
4. O'connor, A. and P. Setlur, "Single-sensor RF emitter localization based on multipath exploitation," *IEEE Transactions on Aerospace and Electronic Systems*, Vol. 51, No. 3, 1635–1651, 2015.
5. Linnehan, R., "Validating multipath responses of moving targets through urban environments," *2010 IEEE Radar Conference*, 1036–1041, IEEE, 2010.
6. Setlur, P., T. Negihi, N. Devroye, and D. Erricolo, "Multipath exploitation in non-LOS urban synthetic aperture radar," *IEEE J. Sel. Topics Signal Process*, Vol. 8, No. 1, 137–152, 2014.
7. Johansson, T., A. Orbom, A. Sume, et al., "Radar measurements of moving objects around corners in a realistic scene," *Radar Sensor Technology*, Vol. 9077, No. 3, 0277-786X, 2014.
8. Sume, A., M. Gustafsson, M. Herberthson, et al., "Radar detection of moving targets behind corners," *IEEE Transactions on Geoscience and Remote Sensing*, Vol. 49, No. 6, 2259–2267, 2011.
9. Gustafsson, M., "Positioning of objects behind corners using X-band radar," *Proc. 30th URSI Gen. Assem. Sci. Symp.*, 1–4, Istanbul, Turkey, 2011.
10. Zetik, R., M. Roding, and R. S. Thoma, "UWB localization of moving targets in shadowed regions," *6th European Conference on Antennas and Propagation*, 1729–1732, Prague, 2012.
11. Johansson, T., A. Andersson, M. Gustafsson, et al., "Positioning of moving non-line-ofsight targets behind a corner," *IEEE Radar Conference*, 2016.
12. Rabaste, O., E. Colin-Koeniguer, et al., "Around-the-corner radar: Detection of a human being in non-line of sight," *IET Radar, Sensor & Navigation*, Vol. 9, No. 6, 660–668, 2015.
13. Li, S., G. Cui, S. Guo, et al., "On the electromagnetic diffraction propagation model and applications," *IEEE J. Sel. Top Appl. Earth Observations Remote Sensing*, Vol. 13, 884–895, 2020.
14. Linnehan, R. and J. Schindler, "Multistatic scattering from moving targets in multipath environments," *IEEE Radar Conference*, 1–6, Pasadena, CA, 2009.
15. Aubry, A., A. De Maio, G. Foglia, et al., "Diffuse multipath exploitation for adaptive radar detection," *IEEE Transactions on Signal Processing*, Vol. 63, No. 5, 1268–1281, 2015.

16. Baranoski, E. J., "Multipath exploitation radar industry day," presented at the Defense Advanced Research Projects Agency Strategic Technology Office, Arlington, VA, 2007.
17. Durek, J., 'Multipath exploitation radar data collection review," presented at the Defense Advanced Research Projects Agency Strategic Technology Office, Arlington, VA, 2009.
18. Zhao, Q., et al., "Millimeter wave radar detection of moving targets behind a corner," *2018 21st International Conference on Information Fusion (FUSION)*, IEEE, 2018.
19. Du, H., C. Fan, C. Cao, et al., "A novel NLOS target localization method with a synthetic bistatic MMW radar," *2020 IEEE 11th Sensor Array and Multichannel Signal Processing Workshop*, 1–5, Hangzhou, China, 2020.
20. Zetik, R., M. Eschrich, S. Jovanoska, et al., "Looking behind a corner using multipath-exploiting UWB radar," *IEEE Trans. on Aerospace and Electronic Systems*, Vol. 51, No. 3, 1916–1926, 2015.
21. Thai, K., O. Rabaste, et al., "GLRT particle filter for tracking NLOS target in around-the-corner radar," *Proc. IEEE Int. Conf. Acoust., Speech, Signal Process.*, 3216–3220, AB, Canada, 2018.
22. Thai, K., O. Rabaste, J. Bosse, et al., "Around-the-corner radar: Detection and localization of a target in non-line of sight," *2017 IEEE Radar Conference (Radar Conf.)*, 2017.
23. Rabaste, O., et al., "Detection-localization algorithms in the around the-corner radar problem," *IEEE Transactions on Aerospace and Electronic Systems*, Vol. 55, No. 6, 2658–2673, 2019.
24. Fan, S., Y. Wang, G. Cui, et al., "Moving target localization behind L-shaped corner with a UWB radar," *2019 IEEE Radar Conference (Radar Conf.)*, IEEE, 2019.
25. Guo, S., S. Li, G. Cui, et al., "MIMO radar localization of targets behind L-shaped corners," *2020 IEEE 11th Sensor Array and Multichannel Signal Processing Workshop (SAM)*, 1–4, Hangzhou, China, 2020.
26. Setlur, P. and G. Smith, "Target localization with a single sensor via multipath exploitation," *IEEE Transactions on Aerospace and Electronic Systems*, Vol. 48, No. 3, 1996–2014, 2012.
27. Di Vito, A. and G. Morreti, "Probability of false alarm in CA-CFAR device downstream from linear-law detector," *Electron. Lett.*, Vol. 25, No. 25, 1692–1693, 1989.